Crystal Structure and Electron Density of α-Silicon Nitride: Experimental and Theoretical Evidence for the Covalent Bonding and Charge Transfer

Masatomo Yashima,*,† Yoshiaki Ando,† and Yasunori Tabira‡

Department of Materials Science and Engineering, Interdisciplinary Graduate School of Science and Engineering, Tokyo Institute of Technology, Nagatsuta-cho 4259, Midori-ku, Yokohama-shi, Kanagawa, 226-8502, Japan, and Corporate R & D Center, Mitsui Mining & Smelting Co. Ltd., Haraichi 1333-2, Ageo-shi, Saitama, 362-0021, Japan

Received: November 27, 2006; In Final Form: February 8, 2007

Crystal structure and electron-density distribution of α-silicon nitride (α-Si_3N_4, space group: $P31c$) have been investigated by a combined technique of the Rietveld method, the maximum-entropy method (MEM), and MEM-based pattern-fitting of high-resolution synchrotron powder diffraction data. In combination with density functional theory calculations, the present experimental electron-density distribution of the α-Si_3N_4 indicates covalent bonds between Si and N atoms and charge transfer from the Si to N atom. The triangular distribution around the N atoms, which is attributable to the nitrogen sp^2 hybridization for the nearest silicon and nitrogen pairs, was found in both experimental and theoretical electron density distributions. The minimum electron density in an intralayer Si−N bond was a little lower than that in an interlayer bond, which would be responsible for the inequality between elastic constants, $C_{33} > C_{11}$. The present work suggests that the high bulk modulus of the α-Si_3N_4 is attributable to the high minimum electron density of the Si−N bond.

1. Introduction

Silicon nitride (Si_3N_4) continues to attract many researchers because of interesting mechanical and dielectric properties.[1−3] In particular, silicon nitride ceramics exhibit high resistance to wear, corrosion, and thermal shock.[1] They also have excellent mechanical properties at high temperatures.[1] Therefore, they have been regarded as some of the promising materials for use in applications such as engine components,[4] engineering dies, and cutting tools. The excellent mechanical properties would correlate with the chemical bonding between the Si and N atoms in the silicon nitride.

There are two well-established crystalline phases of silicon nitride, α- and β-Si_3N_4.[5] The noncentrosymmetric and slightly less dense α-Si_3N_4 undergoes an irreversible first-order phase transformation into the β phase at high temperatures.[6] The crystal structure of α-Si_3N_4 consists of layers of Si and N atoms along the *c*-axis in the sequence of ...ABCDABCD... (Figure 1), and the β structure has ...ABAB... layers. First-principles calculation has suggested that the α- and β-Si_3N_4 are highly covalent.[7] The crystal structures and unit-cell parameters of α- and β-Si_3N_4 have been extensively studied by some researchers.[8−18] du Boulay et al.[8] investigated the electron-density distribution of β-Si_3N_4 using synchrotron X-ray diffraction data and theoretical calculations. However, to the best of our knowledge, there are no reports on the electron-density distribution of α-Si_3N_4 obtained using experimental diffraction data.

The purpose of this work is to study the electron-density distribution of α-Si_3N_4 using synchrotron powder diffraction data. The electron-density distribution would give us insight into Si−N bonds related to the mechanical properties of silicon nitride. Density functional theory (DFT) is employed to calculate the electron-density distribution and elastic properties. In the present study, the covalent bonding among the Si and N atoms is observed in the experimental electron-density distribution of α-Si_3N_4 for the first time. This work also suggests that the high bulk modulus of the α-Si_3N_4 is attributable to the high electron density in the Si−N bonds.

2. Experimental Section

(1) Sample and Synchrotron Powder Diffraction Experiment. Commercial silicon nitride powders (SN-R10, Ube Industrial Co., Ube, Japan) were utilized for a synchrotron powder diffraction measurement. The synchrotron powder diffraction data were measured at 26 °C using a multiple-detector system[19] on the beamline BL-4B_2 at the Photon Factory, High Energy Accelerator Research Organization (KEK), Tsukuba, Japan. The optical system consisted of a bending-magnet light source, a double-crystal Si(111) monochromator, a focusing cylindrical mirror, a flat specimen rotating at 60 rpm, and a multiple-detector system with a Ge(111) flat analyzer crystal and scintillation counters.[19] A monochromatized X-ray of 1.20490(1) Å was obtained by the Si(111) monochromator. An ionic chamber monitored the intensity of the incident beam. The asymmetric 2θ scan technique was used for data collection: The θ angle was fixed at 7° during the measurement of the whole powder pattern. Scanning parameters were as follows: step interval = 0.0040°, counting time = 3 s, diffraction angle 2θ range from 8.000 to 155.000°.

(2) DFT Calculation. The ab initio total energy program VASP (Vienna Ab initio Simulation Package)[20,21] was employed for calculation of the valence electron-density distribution and elastic properties in α-Si_3N_4. Projector augmented-wave (PAW) potentials were used for Si and N atoms.[22,23] A plane-wave basis set with a cutoff of 500 eV was used. The calculations were performed using the Perdew−Burke−Ernzerhof generalized

* Corresponding author. Phone: +81-45-924-5630. Fax: +81-45-924-5630. E-mail: yashima@materia.titech.ac.jp.
† Tokyo Institute of Technology.
‡ Mitsui Mining & Smelting Co. Ltd.

10.1021/jp0678507 CCC: $37.00
Published on Web 03/21/2007

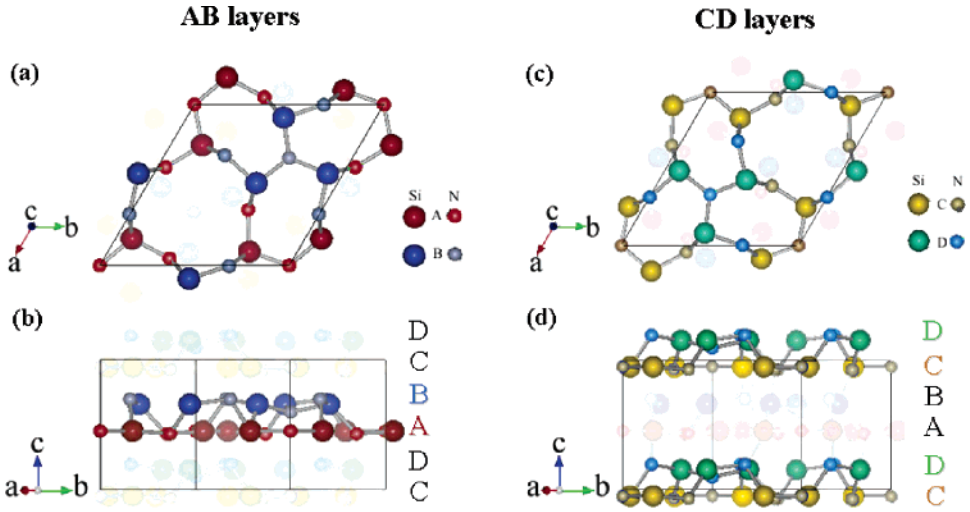

Figure 1. Crystal structure of the α-Si_3N_4 in which the Si−N layers are stacked as ...ABCDABCD.... Projections of the AB layer on the (a) (001) and (b) (100) planes. Projections of the CD layer on the (c) (001) and (d) (100) planes. Solid line stands for the unit cell of the α-Si_3N_4 crystal. These figures were drawn with crystallographic parameters refined in the present work (Table 1).

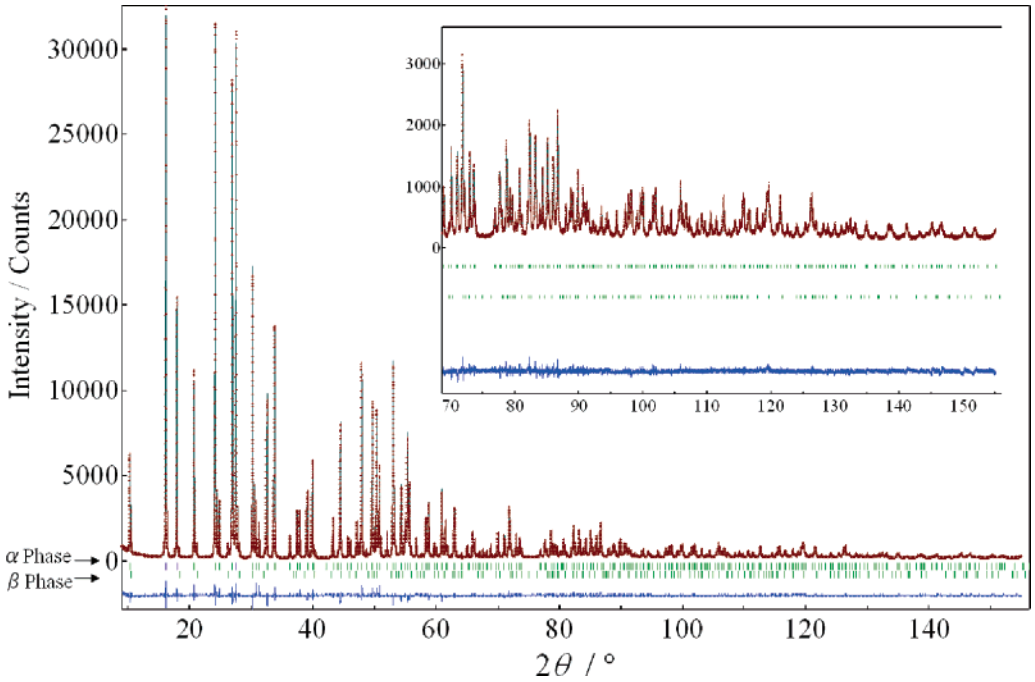

Figure 2. Rietveld fitting result for synchrotron diffraction data of Si_3N_4 powdered sample. Red crosses (+ symbols) and green line denote observed and calculated intensities, respectively. Upper and lower short verticals indicate the positions of possible Bragg reflections of the α- and β-Si_3N_4 phases, respectively. The difference between observed and calculated profiles is plotted at the bottom of the figure.

gradient approximation for the exchange and correlation functional.[24] Sums over occupied electronic states were performed using the Monkhorst−Pack scheme[25] on a 2 × 2 × 3 set of *k*-point mesh. The crystallographic parameters refined using synchrotron data were used for comparison with the experimental results without structural optimization in VASP calculations. Elastic constants were calculated using the VASP. A 0.5% level of strain was applied sequentially for the calculations.

3. Results and Discussion

All the reflection peaks in the synchrotron powder diffraction pattern of the present silicon nitride powders were indexed by the α- and β-Si_3N_4 phases (Figure 2). The experimental data were analyzed by a combination of the Rietveld analysis,[26] the maximum-entropy method (MEM)[27−31] and the MEM-based pattern fitting (MPF).[28−31] It is well-known that the MEM can produce an electron density distribution map from the X-ray diffraction data. In the MEM analysis, any kind of complicated electron density distribution is allowed as long as it satisfies the symmetry requirements.[27−31]

First Rietveld analysis was carried out using the crystallographic parameters reported by Toraya[18] and du Boulay et al.[8] for the α- and β-Si_3N_4 phases, respectively, as initial parameters, using a computer program RIETAN-2000.[26] Space groups $P31c$ and $P6_3/m$ were assumed for the α- and β-Si_3N_4, respectively. The isotropic harmonic model was used for all the atomic displacement parameters. The calculated profile agreed well with the observed intensity data (Figure 2). The refined crystallographic parameters and reliability factors are shown in Table 1. Weight fractions of α- and β-Si_3N_4 calculated using the refined crystallographic parameters and scale factors were 0.975 and 0.025, respectively. The refined unit-cell and

TABLE 1: Refined Crystallographic Parameters and Reliability Factors in the Rietveld, MEM and MPF Analyses of the Synchrotron Diffraction Data of Si_3N_4 Powders[a]

atom	site	structural parameters[b] of α-Si_3N_4 *P*31*c*			
		x	*y*	*z*	*U* (Å^2)
Si	Si1 6*c*	0.08194(4)	0.51161(4)	0.65788(6)	0.0052(5)
	Si2 6*c*	0.25362(4)	0.16730(4)	0.45090	0.0045(5)
N	N1 6*c*	0.65368(9)	0.6100 1)	0.4301(2)	0.0113(5)
	N2 6*c*	0.3159(1)	0.3189(1)	0.6974(2)	0.0093(5)
	N3 2*b*	1/3	2/3	0.5990(2)	0.0059(6)
	N4 2*a*	0.0	0.0	0.4502(3)	0.0095(6)
space group, unit-cell parameter and reliability factors in the Rietveld analysis		R_{wp}=5.41%, R_p=4.01%, goodness of fit, R_{wp}/R_e=1.34			
reliability factors in the second MEM and second MPF analysis		space group of α-Si_3N_4: *P*31*c*; $a = b = 7.7545(1)$ Å, $c = 5.62145(6)$ Å, $\alpha = \beta = 90°$, $\gamma = 120°$, $R_I = 1.86\%$, $R_F = 1.26\%$ (α-Si_3N_4)			
		space group of β-Si_3N_4: $P6_3/m$; $a = b = 7.6069(4)$ Å, $c = 2.9073(1)$ Å, $\alpha = \beta = 90°$, $\gamma = 120°$, $R_I = 2.07\%$, $R_F = 1.05\%$ (β-Si_3N_4)			
		$R_F = 0.86\%$, $wR_F = 0.73\%$ (α-Si_3N_4, second MEM)			
		$R_I = 1.03\%$, $R_F = 0.74\%$ (α-Si_3N_4, second MPF)			
		$R_I = 1.05\%$, $R_F = 0.59\%$ (β-Si_3N_4, second MPF)			

[a] All the occupancy factors are unity. [b] *x*, *y*, and *z* are fractional coordinates of atomic position; *U*, the isotropic atomic displacement parameter.

positional parameters agreed with those reported in the literature.[8,14,18] The refined crystal structure of α-Si_3N_4 consisted of two types of Si−N layers: AB and CD layers. The sequence of the layers along the *c*-axis of the α-Si_3N_4 was confirmed to be ...ABCDABCD... as shown in Figure 1. A Si atom coordinates with four N atoms, forming a SiN_4 tetrahedron. A nitrogen atom is coordinated with three silicon atoms, forming a NSi_3 triangle. These features suggest silicon sp^3 and nitrogen sp^2 hybridizations for the nearest silicon and nitrogen pairs.

Second, the MEM analysis was carried out for the α-Si_3N_4 phase using the structure factors obtained by the Rietveld analysis. The number of structure factors derived in the Rietveld analysis was 449. The MEM calculations were performed using a computer program PRIMA,[28] with 78 × 78 × 56 pixels. To reduce the bias imposed by the simple structural model, an iterative procedure named the REMEDY cycle[28] was employed after the MEM analysis. In the second REMEDY cycle, the *R* factor based on the Bragg intensities, R_I, was improved from 1.86 to 1.03% for the α-Si_3N_4 (see Table 1). *R* factors based on the structure factor, R_F, were also improved by the REMEDY cycle from 1.26 to 0.74% (Table 1).

The MEM electron density map obtained after the REMEDY cycle provided much information on the complicated electron-density distribution (Figures 3 and 4a), as compared with the simple atomic model (Figure 1). Figure 4b shows the projected valence electron-density distribution based on the DFT calculations, which is consistent with the projected experimental density map in Figure 4a. Electron density maps indicate a covalent bonding between Si and N atoms. Both the AB and CD layers form two-dimensional networks of covalent bonding (Figures 3 and 4). The electron-density distribution is not spherical around the nitrogen atoms, as shown in both experimental and theoretical results (Figures 4a and b). The triangular distribution around N atoms is attributable to the nitrogen sp^2 hybridization for the nearest silicon and nitrogen pairs. Tetrahedral distribution of electron clouds around Si atoms is attributable to the silicon sp^3 hybridization for the nearest Si and N pairs.

To evaluate the strength of a certain bond, the minimum electron density was estimated for each Si−N bond, as shown in Table 2. The bond length was also calculated from the refined unit-cell and positional parameters (Table 2). The minimum electron density in a Si−N bond decreases with an increase in the bond length (Figure 5). The minimum electron density in

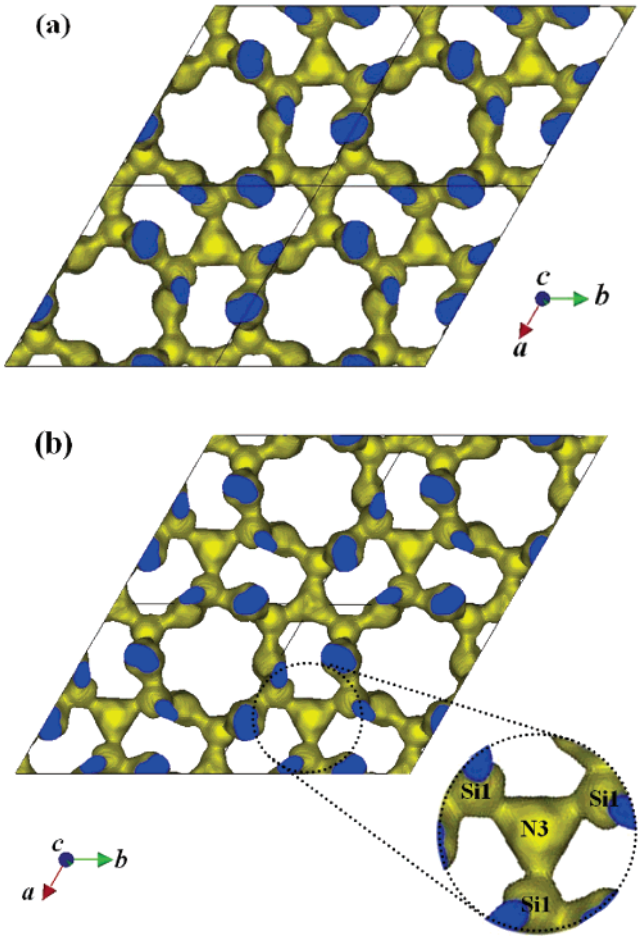

Figure 3. Equidensity surfaces at 0.8 Å^{-3} of electron density on the ***a*−*b*** plane of α-Si_3N_4: (a) AB layer ($0.32 < z < 0.82$) and (b) CD layer ($-0.18 < z < 0.32$). Solid line stands for the unit cell of the α-Si_3N_4 crystal. The inset shows the electron density distribution around the N3 site.

an intralayer Si−N bond was ranged from 1.05 to 1.32 Å^{-3} (average value = 1.1 Å^{-3}), whereas that in an interlayer bond was a little higher (1.14−1.37 Å^{-3}, average value = 1.3 Å^{-3}). Table 3 shows the elastic properties calculated with the VASP program using the refined crystallographic parameters. The elastic constant C_{33} of the α-Si_3N_4 (574 GPa) is a little higher

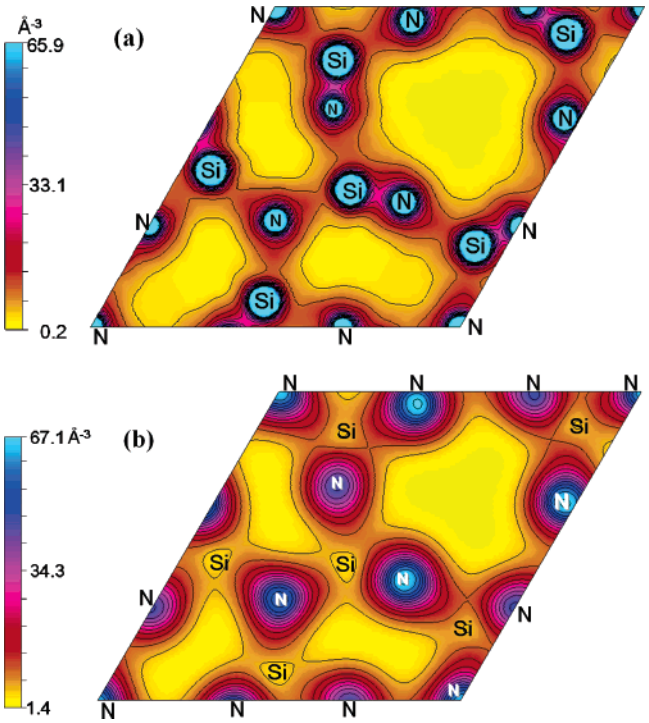

Figure 4. Projected MEM and valence electron density distributions of the AB layer in α-Si_3N_4 ($0.3 < z < 0.7$) obtained through (a) MEM analysis of synchrotron diffraction data and (b) DFT calculations. Contour lines from 6 to 40 $Å^{-3}$ by steps of 5 $Å^{-3}$.

TABLE 2: Minimum Electron Density and Bond Length of Si−N Bonding in α-Si_3N_4

bond[a]	place of bond	minimum electron density ($Å^{-3}$)	bond length (Å)
	Interlayer Bonds		
Si1−N1^{ii}	B−A or D−C interlayer	1.30	1.727(1)
Si1−N1^{i}	B−C or D−A interlayer	1.14	1.743(1)
Si2−N2	A−B or C−D interlayer	1.37	1.723(1)
Si2−N2^{iii}	A−D or C−B interlayer	1.37	1.740(4)
av		1.3(1)	1.733(10)
	Intralayer Bonds		
Si1−N2^{ii}	B or D layer	1.05	1.7414(7)
Si1−N3	B or D layer	1.11	1.7354(4)
Si2−N1^{i}	A or C layer	0.93	1.7506(7)
Si2−N4	A or C layer	1.32	1.7320(2)
av		1.1(2)	1.740(8)
av		1.2(1)	1.74(9)

[a] Symmetry code and operation: (*i*) *x*, *y*, *z*; (*ii*) $-y$, $x-y$, *z*; (*iii*) *y*, *x*, $1/2 + z$; (*iv*) $x-y$, $-y$, $1/2 + z$.

than the C_{11} (526 GPa), which shows reasonable agreement with the literature.[32−35] The difference in the minimum electron density between the interlayer and intralayer Si−N bonds is consistent with the inequality $C_{33} > C_{11}$.

The average value of the minimum electron density of all the Si−N bonds in the α-Si_3N_4 was estimated to be 1.2(1) $Å^{-3}$ (Table 2), which is higher than that of the Si−Si bond in silicon[27] (0.5−0.69 $Å^{-3}$). The bulk modulus of the α-Si_3N_4 (256 GPa in this study (Table 3), 229−248 GPa in the literature[35,36]) is also higher than that of silicon (100 GPa[37]). These results suggest that the high bulk modulus of the α-Si_3N_4 is attributable to the high minimum electron density of the Si−N bond.

To investigate the bonding nature of α-Si_3N_4 in more detail, we calculated the charges around the Si and N sites using the experimental electron-density map. Here, the charges were calculated from the total electronic charges enclosed in spheres around these sites. The radii of the spheres were chosen so as

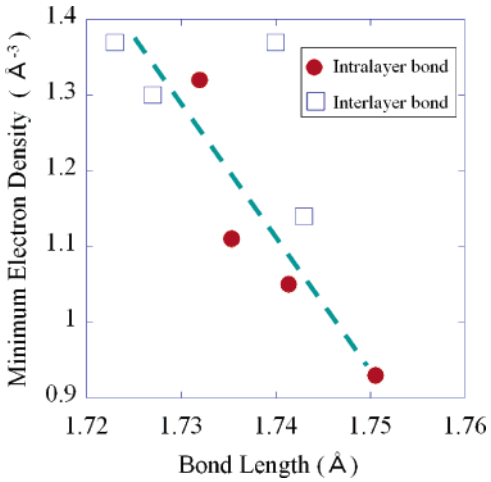

Figure 5. Relationship between the bond length and the minimum electron density of a bond in α-Si_3N_4. Filled circle and open square stand for the intralayer and interlayer bonds, respectively. The dashed line is a guide for the eye.

TABLE 3: Elastic Constants of α-Si_3N_4 Calculated by ab Initio Numerical Procedure

elastic constants (GPa)			modulus
C_{11}	526	bulk modulus (GPa)	256
C_{33}	574	shear modulus	199
C_{12}	128	Young's modulus	473
C_{13}	106	longitudinal modulus	521
C_{14}	185		

to touch both spheres at the density minimum position of the Si−N bond. Atomic charges around the Si1, Si2, N1, N2, N3, and N4 sites were estimated to be 10.08, 10.18, 7.52, 7.99, 7.89, and 7.71, respectively, through the MEM charge density. The average number of electrons around a Si site was 10.1, which was lower than that for the neutral Si atom, 14.0. On the contrary, the average number of electrons around a N site was estimated to be 7.8, which was higher than that for the neutral N atom, 7.0. These results give direct experimental evidence for charge transfer from the Si to N atoms in α-Si_3N_4.

The charge density is pulled from silicon atoms toward nitrogen atoms, as shown in the DFT valence electron-density map (Figure 4b). At the silicon sites, the DFT valence electron density is extremely low (ca. -0.2 $Å^{-3}$), whereas that at the nitrogen sites is high (ca. 3.9 $Å^{-3}$). We calculated the charges around the Si and N sites using the DFT valence-electron-density map. Here, the charges were calculated from the total valence electronic charges enclosed in spheres around these sites. The radii of spheres used were the same as those for the experimental electron-density map. Atomic valence charges around the Si1, Si2, N1, N2, N3, and N4 sites were estimated to be 0.07, 0.07, 6.71, 6.75, 6.72, and 6.29, respectively, through the DFT valence charge density. Thus, the average numbers of electrons around the silicon and nitrogen atoms are estimated to be ∼10.1 and 8.6, respectively, which agree with those (10.1 and 7.8) obtained in the experimental electron-density map.

The present MEM electron density and DFT valence charge density of α-Si_3N_4 have indicated the charge transfer from the silicon atoms to nitrogen atoms. This is mainly ascribed to the difference in the electronegativity. The nitrogen atom is more electronegative than the silicon atoms. This work has also demonstrated that the α-Si_3N_4 has covalent bonding among the silicon and nitrogen atoms (Figures 3 and 4). Therefore, the present study gives experimental and theoretical evidence for the ionic and covalent character in the α-Si_3N_4.

Acknowledgment. We thank Dr. T. Yamada for supplying the silicon nitride powders and Dr. M. Tanaka, Mr. K. Ohuchi, Mr. S. Kobayashi, Mr. W. Nakamura, and Mr. T. Tsuji for experimental assistance. We also thank Mr. K. Chiba for useful discussions. This research was supported in part by the Ministry of Education, Science, Sports and Culture of Japan, Grant-in-Aid. Figures 1, 3, and 4 were drawn using the computer program Venus developed by Dr. R. Dilanian and Dr. F. Izumi.

Note Added after ASAP Publication. This paper was published ASAP on March 21, 2007. A change was made to a heading in Table 2. The updated paper was reposted on March 22, 2007.

References and Notes

(1) Petzow, G.; Herrmann, M. *High Performance Non-Oxide Ceramics II*; Jansen, M., Ed.; Springer: Berlin, 2002; pp 47−167.
(2) Zhao, G. N.; Bachlechner, M. E. *Phys. Rev. B: Condens. Matter Mater. Phys.* **1998**, *58*, 1887−1895.
(3) de Brito Mota, F.; Justo, J. F.; Fazzio, A. *Phys. Rev. B: Condens. Matter Mater. Phys.* **1998**, *58*, 8323−8328.
(4) Lenoe, E. M.; Meglen, J. L. *Am. Ceram. Bull.* **1985**, *64*, 271−275.
(5) Grün, R. *Acta Crystallogr., B: Struct. Sci.* **1979**, *35*, 800−804.
(6) Thompson, D. P. *Mater. Sci. Forum* **1989**, *47*, 21−42.
(7) Xu, Y.-N.; Ching, W. Y. *Phys. Rev. B: Condens. Matter Mater. Phys.* **1995**, *51*, 17379−17389.
(8) du Boulay, D.; Ishizawa, N.; Atake, T.; Streltsov, V.; Furuya, K.; Munakata, F. *Acta Crystallogr., B: Struct. Sci.* **2004**, *60*, 388−405.
(9) Turkdogan, E. T.; Billis, P. M.; Tippett, V. A. *J. Appl. Chem.* **1958**, *8*, 296−302.
(10) Hardie, D.; Jack, K. H. *Nature* (*London*) **1957**, *180*, 332−333.
(11) Ruddlesden, S. N.; Popper, P. *Acta Crystallogr.* **1958**, *11*, 465−468.
(12) Marchand, R.; Laurent, Y.; Lang, J. *Acta Cryst. B: Struct. Sci.* **1969**, *25*, 2157−2160.
(13) Kohatsu, I.; McCauley, J. W. *Mater. Res. Bull.* **1937**, *9*, 917−920.
(14) Kato, K.; Inoue, Z.; Kijima, K.; Kawada, I.; Tanaka, H.; Yamane, T. *J. Am. Ceram. Soc.* **1975**, *58*, 90−91.
(15) Billy, M.; Labbe, J.; Selvaraj, A. *Mater. Res. Bull.* **1983**, *18*, 921−934.
(16) Schneider, J.; Frey, F.; Johnson, N.; Laschke, K. *Z. Kristallogr.* **1994**, *209*, 328−333.
(17) Yang, P.; Fun, H.; Rahman, I. A.; Saleh, M. I. *Ceram. Int.* **1995**, *21*, 137−142.
(18) Toraya, H. *J. Appl. Crystallogr.* **2000**, *33*, 95−102.
(19) Toraya, H.; Hibino, H.; Ohsumi, K. *J. Synchrotron Radiat.* **1996**, *3*, 75−83.
(20) Kresse, G.; Hafner, J. *Phys. Rev. B: Condens. Matter Mater. Phys.* **1993**, *47*, R558−R561.
(21) Kresse, G.; Furthmuller, J. *Phys. Rev. B: Condens. Matter Mater. Phys.* **1996**, *54*, 11169−11186.
(22) Kresse, G.; Joubert, D. *Phys. Rev. B: Condens. Matter Mater. Phys.* **1999**, *59*, 1758−1775.
(23) Blöchl, P. E. *Phys. Rev. B: Condens. Matter Mater. Phys.* **1994**, *50*, 17953−17979.
(24) Perdew, J.; Burke, K.; Ernzerhof, M. *Phys. Rev. Lett.* **1996**, *77*, 3865−3868.
(25) Monkhorst, H. J.; Pack, J. D. *Phys. Rev. B: Condens. Matter Mater. Phys.* **1976**, *13*, 5188−5192.
(26) Izumi, F.; Ikeda, T. *Mater. Sci. Forum* **2000**, *321−324*, 198−203.
(27) Takata, M.; Nishibori, E.; Sakata, M. *Z. Kristallogr.* **2001**, *216*, 71−86.
(28) Izumi, F.; Dilanian, R. A. *Recent Res. Dev. Phys.* **2002**, *3*, 699−726.
(29) Yashima, M.; Tsunekawa, S. *Acta Crystallogr., B: Struct. Sci.* **2006**, *62*, 161−164.
(30) Yashima, M.; Xu, Q.; Yoshiasa, A.; Wada S. *J. Mater. Chem.* **2006**, *16*, 4393−4396.
(31) Yashima, M.; Lee, Y.; Domen, K. *Chem. Mater.* **2007**, *19*, 588−593.
(32) Wendel, J. A.; Goddard, W. A., III *J. Chem. Phys.* **1992**, *97*, 5048.
(33) Ching, W.-Y.; Xu, Y.-N.; Gale, J. D.; Rühle, M. *J. Am. Ceram. Soc.* **1998**, *81*, 3189−3196.
(34) Ogata, S.; Hirosaki, N.; Kocer, C.; Shibutani, Y. *Acta Mater.* **2004**, *52*, 233−238.
(35) Yeheskel, O.; Gefen, Y. *Mater. Sci. Eng.* **1985**, *71*, 95−99.
(36) Kruger, M. B.; Nguyen, J. H.; Li, Y. M.; Caldwell, W. A.; Manghnani, M. H.; Jeanloz, R. *Phys. Rev. B: Condens. Matter Mater. Phys.* **1997**, *55*, 3456−3460.
(37) Kaye, C.; Laby, T. H. *Tables of Physical and Chemical Constants*; Longman; London, 1986.